Meteoritics & Planetary Science 37, 987–1000 (2002)
Available online at http://www.uark.edu/meteor

An experimental and petrographic investigation of Elephant Moraine 79001 lithology A: Implications for its petrogenesis and the partitioning of chromium and vanadium in a martian basalt

CHRISTOPHER D. K. HERD[1]*, CRAIG S. SCHWANDT[2], JOHN H. JONES[3] AND JAMES J. PAPIKE[4]

[1]Lunar and Planetary Institute, 3600 Bay Area Boulevard, Houston, Texas 77058, USA
[2]Lockheed-Martin, Mail Code C23, 2400 NASA Road One, Houston, Texas 77058, USA
[3]Astromaterials Research Office, SR, NASA Lyndon B. Johnson Space Center, Houston, Texas 77058, USA
[4]Institute of Meteoritics, Department of Earth and Planetary Sciences, University of New Mexico, Albuquerque, New Mexico 87131-1126, USA
*Correspondence author's e-mail address: herd@lpi.usra.edu

(Received 2001 December 3; accepted in revised form 2002 April 29)

Abstract–A composition approximating the lithology A groundmass of the Elephant Moraine (EET) 79001 martian basalt (Eg; McSween and Jarosewich, 1983) has been used to investigate the petrogenesis of the meteorite and the behavior of Cr and V at different oxygen fugacities. Crystallization experiments were carried out over a range of temperatures, and oxygen fugacities of either iron–wüstite (IW) or IW + 2 (*i.e.*, 1.5 log units below the quartz–fayalite–magnetite (QFM) buffer). Comparison of trace element concentrations (obtained by secondary ion mass spectrometry (SIMS) analysis) in experimental silicates with those of natural silicates supports the Fe-Ti oxide-derived oxygen fugacity of QFM −1.8 ± 0.3 for this basalt (Herd *et al.*, 2001). Experimental distribution coefficients, in conjunction with SIMS analyses of rims from the olivine and pyroxene xenocrysts in lithology A, as well as analyses of lithology A groundmass pigeonite cores, are used to calculate coexisting liquid concentrations of V and Cr. Liquid compositions derived from pigeonite xenocryst rims and groundmass pigeonite cores are similar, suggesting that the rims of orthopyroxene xenocrysts are overgrowths, which have not previously been accounted for when reconstructing the groundmass composition. This implies that the Eg composition requires modification. A similar exercise for the ferroan rims on olivine xenocrysts yields very different liquid compositions, indicating that these rims are not overgrowths but are part of the xenocryst assemblage. These results are shown to be consistent with the petrography of lithology A xenocrysts.

INTRODUCTION

The Elephant Moraine (EET) 79001 martian meteorite contains two lithologies in igneous contact: lithology A, which is composed of xenocrysts of low-Ca pyroxene, olivine, and Cr-spinel in a fine-grained (0.15 mm) basaltic groundmass; and lithology B, which is composed of a coarser-grained (0.30 mm) basalt similar to Shergotty (Steele and Smith, 1982). A synthetic martian basaltic magma with the composition of the groundmass of EET 79001 lithology A has been used in a number of experiments to constrain martian parental magmas and to investigate the nature of martian basaltic magmatism (Longhi and Pan, 1989; Wasylenki *et al.*, 1993). This composition, referred to as "Eg" (McSween and Jarosewich, 1983; Longhi and Pan, 1989), was calculated by subtracting weight fractions of xenolithic olivine and pyroxene from the bulk lithology A composition, using averages of xenocryst core and rim compositions (McSween and Jarosewich, 1983). The assumption was made that olivine and pyroxene in the xenoliths were already zoned before incorporation into the groundmass (McSween and Jarosewich, 1983). However, the amount of interaction between the xenoliths and the groundmass is not well known, calling into question the exact nature of EET 79001 lithology A (Mittlefehldt *et al.*, 1999). McSween and Jarosewich (1983) suggested that lithology A is a mixture of lithology B and the harzburgitic xenolith lithology, which is similar to the poikilitic domains in the Allan Hills 77005 meteorite. But the caloric difficulties of a lower temperature melt such as lithology B assimilating a harzburgite to become a higher temperature melt like lithology A are difficult to overcome (Wadhwa *et al.*, 1994). One means of circumventing these difficulties is if lithology A represents an impact melt (Mittlefehldt *et al.*, 1999), which has been heated above its liquidus.

Prelude preprint MS#4705

The purpose of this study was to address some of these petrogenetic questions regarding lithology A. In particular, we have experimentally investigated the partitioning behaviors of Cr and V, which are redox-sensitive elements. Chromium exists as Cr^{2+} and Cr^{3+} and V as V^{3+} and V^{4+} at terrestrial oxygen fugacities (Canil, 1997, 1999), approximately QFM –3 to QFM +4 (quartz–fayalite–magnetite buffer; after Wones and Gilbert, 1969). Our goals were that these experiments would evaluate oxygen fugacities that had been previously determined for EET 79001 using Fe-Ti oxides (QFM –1.8 ± 0.3; Herd *et al.*, 2001) and also better constrain which of the various components of lithology A were in equilibrium with the groundmass composition. To these ends, we will use major, minor, and trace element comparisons between experimental and natural mineral compositions to investigate the origin of lithology A and the relationship between the groundmass and the xenoliths.

EXPERIMENTAL AND ANALYTICAL DETAILS

Starting Compositions

A composition matching that of Eg of Longhi and Pan (1989), in terms of all elements except Cr was synthesized using reagent-grade oxide powders. The Cr_2O_3 concentration of 0.15 wt% (~1000 ppm Cr) for the Eg liquid was initially calculated from an assumed $D_{Cr}^{pig/liq}$ of 3 and pyroxene core compositions (Mittlefehldt, unpubl. data). For comparison, the Cr_2O_3 content of previous estimates (McSween and Jarosewich, 1983; Longhi and Pan, 1989) is 0.12 wt%, or ~820 ppm Cr. However, our Cr content is considerably lower than would be estimated from the modal abundance of pyroxene (Mittlefehldt, pers. comm., 2001). Our chosen Cr content also corresponds to the approximate spinel saturation point, for an oxygen fugacity of QFM –1.5 and a temperature of 1200 °C, as determined for mid-ocean ridge basalts (MORB) by Hanson and Jones (1998).

Our Eg V concentration is based on the measured V concentration of groundmass low-Ca pyroxene cores, which averages ~200 ppm (Wadhwa, unpubl. Ph.D. thesis). The bulk rock (lithology A) contains between 210 and 230 ppm V (Meyer, 1998), suggesting a D value for V in low-Ca pyroxene of nearly unity.

The appropriate amounts of Cr_2O_3 and V_2O_5 were measured and added to a powdered glass of Eg composition of Wasylenki *et al.* (1993). The mixture was ground with an agate mortar and pestle, under acetone, for 20 min to ensure homogeneity. Table 1 presents the starting composition, including measured Cr and V content by secondary ion mass spectrometry (SIMS) and electron microprobe (EMP). Experiments were carried out at two oxygen fugacities, that of the assumed oxygen fugacity of crystallization, QFM –1.5, and under more reducing conditions, around the iron–wüstite (IW) buffer (approximately QFM –3.5).

TABLE 1. Elephant Moraine 79001 lithology A parental melt compositions.

Wt%	Eg5/6*	Eg†	Eg‡	Eg§
SiO_2	50.4 ± 0.2	50.67	49.20	49.0
TiO_2	0.85 ± 0.01	0.86	0.78	1.7
Al_2O_3	7.20 ± 0.02	7.10	6.44	7.4
FeO	18.8 ± 0.2#	18.67	18.49	18.4
MgO	12.23 ± 0.04	12.22	14.40	11.5
MnO	0.50 ± 0.005	0.52	0.51	0.52
CaO	8.90 ± 0.04	8.74	7.96	9.2
K_2O	–	0.07	0.06	0.0
Na_2O	0.94 ± 0.02	1.07	0.97	0.9
P_2O_5	–	–	–	1.2
Cr_2O_3	0.154 ± 0.005	0.12	0.12	0.15
V_2O_3	0.042 ± 0.002	–	–	0.03
Total	100.08	100.04	98.93	100.0
SIMS analysis for Cr and V$				
Cr_2O_3		0.138 ± 0.011		
V_2O_3		0.032 ± 0.001		

*Carried out using the SX-100 at JSC; reported error is the standard deviation of 10 analyses.
†Longhi and Pan (1989).
‡McSween and Jarosewich (1983).
§Preferred Eg composition based on observations in this study.
#FeO content is measured after addition of FeO to compensate for loss to Pt loop.
$SIMS analysis at UNM; reported error is the standard deviation of 5 analyses.

Platinum-Loop Gas-Mixing Experiments at 1 Bar, Oxygen Fugacity = QFM –1.5

Pt-loop gas-mixing experiments were performed in Deltech furnaces at the Johnson Space Center (JSC). Two sets of experiments were run at an oxygen fugacity of 1.5 log units below QFM. The first involved addition of Cr to the Eg composition (referred to as Eg5), and the second, addition of V to Eg5 (referred to as Eg6). Thus, all Eg5 experiments for Cr at QFM –1.5 were repeated. A test run was performed at 1350 °C to determine the homogeneity of Cr and V (Table 1) and the amount of Fe loss to the Pt loop. Cr and V were found to be homogeneous within analytical error (Table 1). About 1.1 wt% FeO was lost to the Pt10Rh loop. This was compensated for by adding 1.2 wt% Fe_2O_3 to subsequent runs (Table 1). We were able to demonstrate that our experiments did not gain or lose FeO relative to the starting composition by performing mass-balance calculations based on EMP analyses of glass and crystals.

Oxygen fugacity was controlled by mixing CO and CO_2 and measured using a ZrO_2 sensor in an external calibration furnace. Oxygen fugacity is accurate to within ±0.2 log units

(Jurewicz *et al.*, 1993). Charges were made by pressing ~125 mg of material into a pellet, which was fused to the Pt loop with a propane torch. Charges were homogenized at 1350 °C for 24 h before being lowered to temperature at a rate of 1000 °C/h, and held in the calibrated hot spots of the furnaces at 1250, 1200 or 1150 °C. Temperature was measured with a type-B thermocouple calibrated against the melting point of Au. The charges were held at temperature for 48 h and then quenched in air.

An additional experimental run was carried out in a Deltech furnace at the experimental petrology laboratory at the University of New Mexico (UNM), Department of Earth and Planetary Sciences. Oxygen fugacity was controlled by mixing H_2 and CO_2 and measured with an internal ZrO_2 oxygen fugacity sensor. About 70 mg of Eg6 composition was fused onto the Pt10Rh loop, homogenized at 1350 °C for 24 h, lowered to temperature at a rate of 900 °C/h, held at 1200 °C for 48 h, and then quenched in air.

Rhenium-Loop Gas-Mixing Experiments at 1 Bar, Oxygen Fugacity = IW

Re-loop gas-mixing experiments were performed in Deltech furnaces at JSC. Experiments employed the Eg6 composition, containing both Cr and V. Correction for Fe loss was not required due to the lack of uptake of Fe by Re (Borisov and Jones, 1999). Fe loss was again demonstrated to be insignificant, by mass-balance calculations as described above. Re will oxidize in air (Borisov and Jones, 1999), precluding the use of a propane torch to fuse material to the Re loop. Instead, the Eg6 material was mixed with polyvinyl alcohol to make a paste that could be formed into a ball and stuck to the Re loop. This was allowed to dry before being placed in the furnace. Oxygen fugacity and temperature were controlled as described previously for the experiments carried out at JSC.

Analytical Methods

Elemental Analysis by Electron Microprobe–Major and minor element analysis of phases in the experimental charges and natural pyroxene was performed using the JEOL-733 EMP at the UNM, Department of Earth and Planetary Sciences Microbeam Facility, equipped with five wavelength dispersive spectrometers at an accelerating voltage of 15 kV and a beam current of 20 nA. Well-known silicate standards were used. Counting times for major elements including Si, Al, Mg, Fe, and Ca, as well as the minor elements Ti, K and Na were 20 s on the peak, 10 s on each background. Manganese was analyzed using counting times of 30 s on the peak, 10 s on each background. Cr was analyzed using counting times of 40 s on the peak, 20 s on each background. This resulted in adequate count rates (10^2 s^{-1} to 10^3 s^{-1} for major elements; 10^1 s^{-1} for minor elements).

Elemental Analysis by Ion Microprobe–Analysis of V and Cr in experimental charges and natural pyroxene was conducted using the Cameca IMS 4f ion microprobe operated on the UNM campus by UNM and Sandia National Laboratories. Analyses were made by bombardment of the sample with primary O^- ions accelerated through a nominal potential of 10 or 12.5 kV. A primary ion current of 15 nA was focused on the sample over a spot diameter of 15 or 20 μm. Target areas were carefully selected using ion imaging, to avoid contamination by other phases. Sputtered secondary ions were energy filtered using sample offset voltages of –105 V and an energy window of 50 V, to eliminate effectively most isobaric interferences. Peak counting times were varied to optimize precision. Absolute concentrations of each element were calculated using empirical relationships of measured peak/$^{30}Si^+$ ratios normalized to known SiO_2 content (from EMP analyses).

Elemental Mapping by Electron Microprobe–To quantitatively evaluate the petrography of lithology A, we made elemental maps of a large thin section using the Cameca SX-100 at JSC. We employed digital wavelength dispersive elemental mapping and software optimized for handling large data arrays (Noesys + IDL). A 6 × 22 mm area of the EET 79001,68 thin section was mapped for 10 elements, with pixel dimensions of 20 × 20 μm, yielding a map with 330 000 points (Schwandt *et al.*, 2001). Beam current was 40 nA and counting time was 65 ms per analysis. Mapping of selected xenocrysts utilized alternate beam conditions in order to optimize acquisition. The olivine xenocryst maps consist of four maps of 400 × 400 pixels (2 μm step size) collected with a 60 nA beam current and 20 ms dwell time per pixel. The pyroxene xenocrysts utilized a 100 nA beam current with 20 ms dwell time per pixel. The final pyroxene map consists of four maps each 500 × 500 μm with a 2 μm step size. Use of the IDL software allows mathematic operations with the element arrays on a pixel-by-pixel basis, such that element ratio maps can be constructed.

RESULTS AND DISCUSSION

Observations

The experimental charges all contain crystals. Olivine crystals in the 1250 °C runs are elongate and often skeletal. Olivine in the 1200 and 1150 °C runs exists as rare, small, anhedral crystals. Pyroxene crystals are elongate and are predominant in the 1200 and 1150 °C runs. No spinel was observed in any of the charges in this study. Crystal sizes (smallest dimension) ranged from 100 to 1000 μm in the 1250 °C runs to 10 to 50 μm in the runs at lower temperatures. Glass was found to be homogenous in all charges within analytical error, in terms of major, minor and trace elements. In the 1250 °C runs, crystals were often large enough to perform core–rim traverses using the SIMS to assess zoning in Cr and V. No zoning was observed in silicates at this temperature at either oxygen fugacity. Core–rim traverses were often not possible in the 1200 and 1150 °C runs due to the small size of crystals.

TABLE 2. Phase compositions from experiments performed at QFM –1.5.

Temperature	Eg5* (1250 °C)	Eg5 (1200 °C)	Eg5 (1150 °C)	Eg6† (1250 °C)	Eg6 (1200 °C)	Eg6 (1200 °C)‡	Eg6 (1150 °C)	
Glass								
SiO_2	52.0(6)	52.7(8)	50.28(8)	52.0(3)	51.1(3)	50.7(3)	51.7(4)	–
TiO_2	0.95(2)	1.04(4)	1.21(1)	0.95(3)	1.13(3)	1.17(4)	1.33(2)	–
Al_2O_3	7.6(2)	8.3(3)	10.13(5)	7.49(7)	8.9(2)	9.6(1)	10.87(6)	–
MgO	9.5(2)	8.2(1)	6.5(1)	10.0(1)	7.8(1)	7.48(5)	5.66(3)	–
MnO	0.52(3)	0.51(1)	0.45(1)	0.54(3)	0.49(3)	0.50(4)	0.46(4)	–
FeO	18.2(3)	18.0(3)	18.45(1)	18.1(2)	18.0(2)	17.9(2)	17.3(2)	–
CaO	10.0(1)	10.8(2)	11.20(7)	9.76(8)	10.8(1)	11.11(8)	10.3(1)	–
Na_2O	1.05(4)	1.17(6)	1.4(2)	0.94(1)	1.00(4)	1.02(2)	2.20(6)	–
K_2O	bdl§	bdl	bdl	bdl	bdl	bdl	bdl	–
Cr_2O_3	0.19(1)	0.14(2)	0.069(7)	0.15(2)	0.11(1)	0.09(2)	0.04(1)	–
Total	100.01	100.86	99.69	99.93	99.33	99.57	99.86	–
mg#	0.48	0.45	0.39	0.50	0.44	0.43	0.37	–
Cr_2O_3#	–	–	–	0.16(3)	0.11(2)	0.09(2)	0.05(1)	–
V_2O_3#	–	–	–	0.036(8)	0.036(8)	0.032(7)	0.027(6)	–
% Glass	89	84	68	95	79	74	65	–
Olivine								
SiO_2	38.4(3)	37.29(8)	36.31(6)	38.2(2)	38.0(2)	36.6(5)	37.0(2)	–
MgO	36.8(4)	35.0(4)	31.33(1)	38.1(2)	34.6(2)	33.9(2)	29.4(5)	–
MnO	bdl	bdl	bdl	–	–	–	–	–
FeO	23.2(3)	26.4(2)	30.1(6)	23.6(3)	26.8(3)	28.0(2)	31.8(2)	–
CaO	0.25(2)	0.32(3)	0.46(2)	0.28(3)	0.32(5)	0.41(4)	0.5(1)	–
Cr_2O_3	0.14(1)	0.13(1)	0.07(1)	0.12(1)	0.10(1)	0.08(2)	0.036(7)	–
Total	98.79	99.14	98.27	100.3	99.82	98.99	98.74	–
K_D	0.33	0.35	0.34	0.35	0.34	0.35	0.36	–
Cr_2O_3#	–	–	–	0.10(2)	0.09(2)	0.16(4)	0.04(1)	–
V_2O_3#	–	–	–	0.0035(7)	0.0041(9)	0.014(3)	0.008(2)	–
% Olivine	11	14	8	5	8	5	12	–
Pyroxene								
SiO_2	–	53.9(2)	52.6(3)	–	53.7(6)	53.3(3)	53.3(8)	52.4(4)
TiO_2	–	0.14(2)	0.18(4)	–	0.11(3)	0.16(3)	0.20(3)	0.33(5)
Al_2O_3	–	0.72(8)	0.9(2)	–	0.7(1)	0.8(1)	0.9(2)	1.5(2)
MgO	–	24.7(2)	22.2(3)	–	24.5(4)	23.9(2)	21.5(4)	17.9(8)
MnO	–	bdl	bdl	–	bdl	bdl	bdl	bdl
FeO	–	16.7(2)	17.8(4)	–	16.4(3)	16.6(2)	18.3(6)	14(1)
CaO	–	3.1(2)	4.9(4)	–	3.3(2)	3.7(3)	5.3(8)	12(2)
Na_2O	–	–	–	–	bdl	bdl	bdl	0.13(3)
Cr_2O_3	–	0.5(1)	0.4(2)	–	0.5(1)	0.4(1)	0.4(1)	0.7(1)
Total	–	99.76	98.98	–	99.21	98.86	99.90	98.96
K_D	–	0.31	0.29	–	0.29	0.29	0.28	0.26
Cr_2O_3#	–	–	–	–	0.39(8)	0.6(1)	0.10(2)	0.36(8)
V_2O_3#	–	–	–	–	0.026(6)	0.039(8)	0.030(6)	0.042(9)
% Px	0	2	24	0	13	21	23$	$
NBO/T	1.27	1.18	1.12	1.28	1.18	1.15	1.00	–

*Eg5 experiments were carried out in March 1999.
†Eg6 experiments were carried out in March 2000.
‡Experiment carried out at UNM.
§bdl = below detection limits.
#From SIMS analysis; see text for details.
$Pigeonite and augite were not distinguished in phase proportion calculations.

However, zoning in terms of Cr and V in the pyroxene in the 1200 °C IW run was observed, with cores containing ~2800 ppm Cr and 130 ppm V and rims containing ~2200 ppm Cr and 99 ppm V. Pyroxene in the 1150 °C QFM –1.5 run was highly variable in composition, ranging from $En_{60}Fs_{30}Wo_{10}$ to $En_{45}Fs_{20}Wo_{35}$. Accordingly, Cr contents of the pyroxene varied from ~2700 to 4900 ppm Cr. Core–rim variations were difficult to assess due to small crystal sizes.

Crystallization of phases at QFM –1.5 is as follows: olivine → low-Ca pyroxene + olivine → low-Ca pyroxene + olivine + high-Ca pyroxene. At IW, the sequence is: olivine + low-Ca pyroxene → low-Ca pyroxene. Olivine does not appear to be as stable at lower temperatures at lower oxygen fugacity. For comparison, Wasylenki *et al.* (1993) observed the following sequence at QFM: olivine → low-Ca pyroxene + olivine → low-Ca pyroxene.

Results of the analyses of the experiments using the Eg5 and Eg6 compositions at QFM –1.5 are given in Table 2. Table 3 presents results of analyses of the Eg6 experiments performed at IW, and Table 4 gives a summary of pyroxene and olivine analyses from EET 79001 lithology A, for comparison.

Loss of Vanadium to the Rhenium Loop?

The V contents of phases are significantly less at IW than at QFM –1.5 (Tables 2 and 3), suggesting V loss in the IW runs. Mass balance calculations show that approximately two-thirds of the 200 ppm V in the composition was lost. Since the loss was independent of final equilibration temperature, it likely occurred during the 24 h homogenization period at 1350 °C. Volatilization of V species is unlikely, so V was probably lost to the Re loop. This could not be verified, however, because of the analytical difficulties in detecting trace amounts of V in Re in thin section. Despite the loss, D_V values are consistent with published values (see below), and V contents of phases were above detection limits. No Cr loss was observed in any of the experiments.

Comparison of Experimental and Natural Compositions

Figure 1 is a plot of experimental and natural pyroxene compositions on the pyroxene quadrilateral. Figure 2 is a comparison of the Mg numbers (*mg#* = molar Mg/(Fe + Mg)) of experimental glasses with calculated *mg#* for coexisting liquid from natural compositions. Liquid *mg#* is calculated using an Fe-Mg exchange K_D of 0.33 for olivine (Walker *et al.*, 1976), and 0.28 for pyroxene (Grove and Bence, 1977). These are in good agreement with the K_D values calculated on the basis of Fe-Mg distribution in the experimental runs (Tables 2 and 3). The figures show an overlap between the Fe-rich pigeonite xenocryst compositions and the experimental pigeonites. There appears to be a continuum between orthopyroxene xenocryst rims (pigeonite) and groundmass pigeonite cores.

TABLE 3. Phase compositions from experiments performed at IW.

Temperature	Eg6 (1250 °C)	Eg6 (1200 °C)	Eg6 (1150 °C)
Glass			
SiO_2	51.3(3)	50.1(6)	50.0(3)
TiO_2	0.99(2)	1.17(2)	1.34(3)
Al_2O_3	8.21(8)	9.41(8)	11.21(8)
MgO	9.9(1)	7.56(9)	6.02(7)
MnO	0.59(4)	0.52(4)	0.46(4)
FeO	17.8(2)	19.3(4)	18.0(2)
CaO	10.5(1)	11.2(1)	11.5(1)
Na_2O	0.38(3)	0.68(2)	1.00(4)
K_2O	bdl*	bdl	bdl
Cr_2O_3	0.14(2)	0.10(2)	0.06(2)
Total	99.81	100.04	99.59
mg#	0.50	0.41	0.37
Cr_2O_3†	0.15(3)	0.11(2)	0.08(2)
V_2O_3†	0.009(2)	0.009(2)	0.007(2)
% Glass	87	75	63
Olivine			
SiO_2	38.0(4)	–	–
MgO	37.1(4)	–	–
MnO	–	–	–
FeO	24.3(2)	–	–
CaO	0.28(3)	–	–
Cr_2O_3	0.11(1)	–	–
Total	99.79	–	–
K_D	0.37	–	–
Cr_2O_3†	0.11(2)	–	–
V_2O_3†	0.0031(7)	–	–
% Olivine	3	0	0
Pyroxene			
SiO_2	54.4(3)	53.6(2)	52.7(5)
TiO_2	0.10(3)	0.15(3)	0.22(6)
Al_2O_3	0.4(1)	0.66(9)	0.9(2)
MgO	27.2(2)	23.9(2)	21.2(5)
MnO	bdl	bdl	bdl
FeO	15.0(2)	17.5(2)	19.0(6)
CaO	2.0(1)	3.5(2)	5.1(4)
Na_2O	bdl	bdl	bdl
Cr_2O_3	0.24(4)	0.32(7)	0.22(5)
Total	99.34	99.63	99.34
K_D	0.31	0.29	0.30
Cr_2O_3†	0.25(6)	0.34(8)	0.24(5)
V_2O_3†	0.008(2)	0.016(4)	0.011(2)
% Px	10	25	37
NBO/T	1.26	1.21	1.05

*bdl = below detection limits.
†From SIMS analysis; see text for details.

TABLE 4. Compositions of pyroxene and olivine in EET 79001 Lithology A.

Oxides	Groundmass pigeonite		Xenocryst orthopyroxene			Xenocryst olivine		
	Core* (wt%)	Rim* (wt%)	Average* (wt%)	Core (wt%)	Rim (wt%)	Average* (wt%)	Core (wt%)	Rim (wt%)
SiO_2	53.3	49.4	54.7	54.9	54.4	38.3	38.5	35.3
TiO_2	0.13	0.62	0.11	bdl†	0.33	0.02	–	–
Al_2O_3	0.64	0.68	0.60	1.27	0.90	0.02	–	–
MgO	21.6	15.7	24.5	29.9	16.5	36.8	38.8	26.2
MnO	0.57	0.84	0.60	0.70	0.36	0.55	–	–
FeO	18.2	27.0	15.2	10.7	21.1	24.0	22.3	37.6
CaO	4.93	5.51	3.03	1.48	5.89	0.26	0.25	0.23
Na_2O	0.06	0.12	0.04	0.02	0.06	0.03	–	–
Cr_2O_3	0.44	0.36	0.49	0.68	0.38	0.07	0.10	0.04
Total	99.87	100.23	99.27	99.23	99.56	100.05	99.95	99.37
Liquid *mg#*	0.37	0.22	0.45	0.58	0.28	0.47	0.51	0.29

*Data from McSween and Jarosewich (1983); all other data from this study.
†bdl = below detection limits.

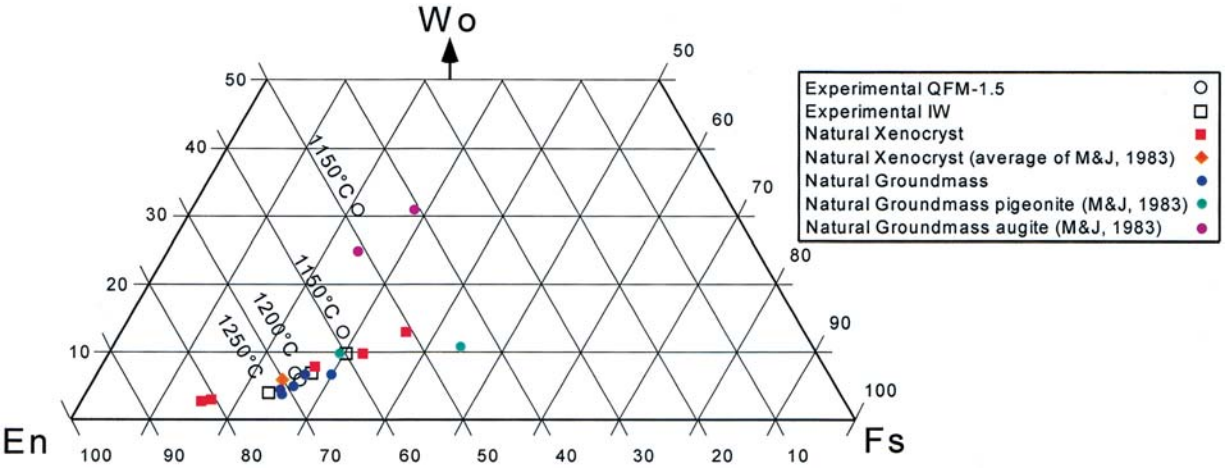

FIG. 1. Pyroxene quadrilateral comparing natural and experimental pyroxene compositions.

Oxygen fugacity has little observable effect on the bulk compositions of pyroxenes. However, the effect on V and Cr partitioning is significant. The Cr and V contents of experimental pyroxenes at QFM –1.5 and natural pyroxenes are similar (Fig. 3). Experimental pyroxenes at QFM –1.5 (average of all temperatures) contain ~0.4 wt% Cr_2O_3, but only 0.26 wt% Cr_2O_3 at IW. Natural pigeonite cores and rims and xenocryst rims have Cr_2O_3 = 0.44 to 0.36 wt% (Table 4). Experimental V contents of orthopyroxenes at QFM –1.5 range from 174 to 263 ppm. Pyroxenes from the IW runs have V contents of 56 to 112 ppm. Natural groundmass cores have an average V content of 177 ppm. Therefore the oxygen fugacity of EET 79001 lithology A as determined by Fe-Ti oxides (QFM –1.8 ± 0.3; Herd *et al.*, 2001) appears justified as a correct parameter for the experiments. Also, these results reinforce the correctness of our choice of Cr and V contents for the starting composition.

Distribution Coefficients

Distribution coefficients for olivine, and low- and high-Ca pyroxene are presented in Table 5. *D* values for Cr derived from EMP analyses are in agreement with those derived from SIMS analyses, except in two cases. In the QFM –1.5, 1200 °C run carried out at UNM, the concentration of Cr in olivine from EMP analysis is in agreement with Cr in olivine from the JSC 1200 °C run at the same oxygen fugacity (Table 2). However, the measured Cr in olivine from SIMS analyses is

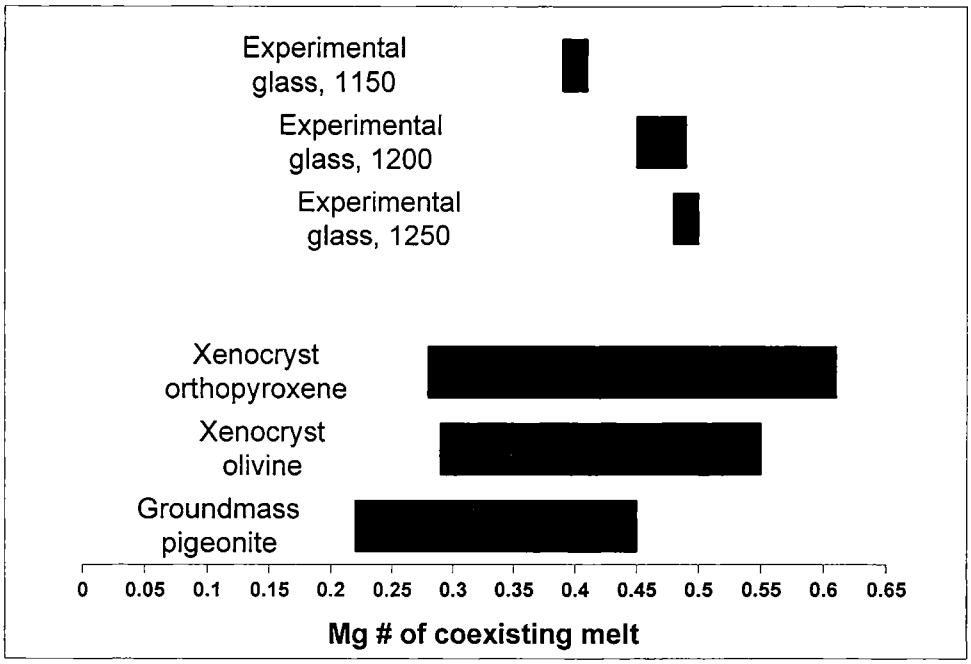

FIG. 2. Comparison of experimental *mg#* of liquid and calculated *mg#* of liquid from natural pyroxene and olivine compositions. *Mg#* of liquid from natural pyroxenes calculated using $K_D = 0.28$ (Grove and Bence, 1977). *Mg#* of liquid from natural olivines calculated using $K_D = 0.33$ (Walker *et al.*, 1976).

twice that from EMP (Table 2). The problem appears to be due to the small size of olivine crystals (~15 μm across) in the UNM 1200 °C run, which, despite our efforts, may have allowed for contamination by pyroxene during SIMS analysis, which has higher concentrations of Cr (Table 2). This contamination was avoided during EMP analysis because of the small size of the electron beam (typically 1–2 μm). Similarly small olivines are present in the equivalent JSC run. These were initially analyzed by SIMS, but the results were discarded in favor of those from a larger crystal. Therefore it

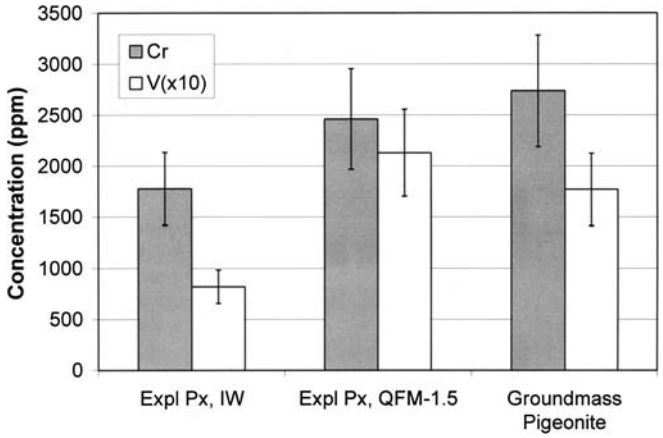

FIG. 3. Comparison of concentrations of Cr and V (multiplied by 10) in experimental pyroxenes and natural pyroxene (groundmass pigeonite) at two oxygen fugacities. Experimental pyroxene concentrations represent the average of all pyroxenes crystallized at that oxygen fugacity. Note the similarity in concentrations between pyroxenes crystallized at QFM –1.5 and groundmass pigeonite.

appears that the D_{Cr}^{Ol} at QFM –1.5 derived from the JSC 1200 °C run is more accurate than the D_{Cr}^{Ol} from the UNM 1200 °C run.

The second discrepancy occurs in the pyroxene of the QFM –1.5, 1150 °C run, which contains variable amounts of Ca and Cr, presumably due to sector zoning. EMP analyses show higher Cr contents than SIMS analyses (Table 2). We attribute this to differences in sampling volume by the two techniques. SIMS analysis likely averaged variable compositions, and appears to underestimate the Cr concentration. Cr concentrations from EMP are highly variable, even in a single crystal, and have accordingly high uncertainties (Table 2). Nevertheless, D_{Cr}^{Cpx} is greater than D_{Cr}^{Opx}, no matter which technique is used. This relationship is expected based on crystal chemical effects.

As noted previously, zoning was observed in the IW, 1200 °C run. The D^{Px} values given in Table 5 are based on average rim concentrations.

Chromium and Vanadium Partitioning into Olivine–Hanson and Jones (1998) showed that D_{Cr}^{Ol} varies with oxygen fugacity and liquid composition, the latter represented by the ratio of non-bridging oxygens to tetrahedral oxygens (NBO/T; Mysen, 1983). At higher oxygen fugacity most of the Cr is Cr^{3+} and D_{Cr}^{Ol} correlates with NBO/T, whereas at lower oxygen fugacity most of the Cr is Cr^{2+} and D_{Cr}^{Ol} correlates with MgO in the liquid. Figure 4a shows that at QFM –1.5 D_{Cr}^{Ol} coefficients from the Eg experiments lie along the Hanson and Jones (1998) trend for D_{Cr3+}^{Ol} *vs.* NBO/T, implying that most of the Cr is Cr^{3+}. However, at IW the one Eg datum lies along the D_{Cr}^{Ol} *vs.* D_{Mg}^{Ol} trend of Hanson and

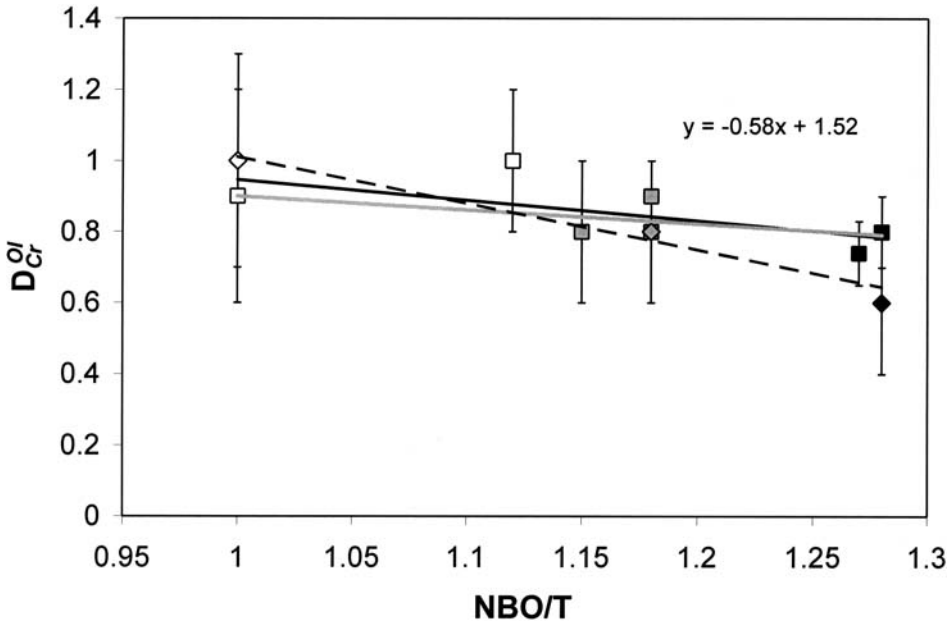

FIG. 4. Effect of oxygen fugacity on Cr partitioning in olivine (a) Plot of D_{Cr}^{Ol} *vs.* NBO/T of melt from experiments at QFM –1.5. Solid black points are data from 1250 °C; gray (center) from 1200 °C and open points from 1150 °C. Regression line to EMP data (squares) is shown as a solid black line, with equation given. Fit to SIMS-derived data (diamonds) is shown as a dashed line. The relationship of Hanson and Jones (1998) is shown as a gray line. These relationships indicate that most of the Cr at this oxygen fugacity is Cr^{3+}.

TABLE 5. Calculated distribution coefficients for V and Cr in the Eg composition.

fO_2 = QFM –1.5	Eg5			Eg6			
Temperature	(1250 °C)	(1200 °C)	(1150 °C)	(1250 °C)	(1200 °C)	(1200 °C)*	(1150 °C)
NBO/T	1.27	1.18	1.12	1.28	1.18	1.15	1.00
D_{Cr}^{Ol} EMP	0.74 ± 0.09	0.9 ± 0.1	1.0 ± 0.2	0.8 ± 0.1	0.8 ± 0.2	0.8 ± 0.2	0.9 ± 0.3
D_{Cr}^{Ol} SIMS	–	–	–	0.6 ± 0.2	0.8 ± 0.2	1.8 ± 0.6	1.0 ± 0.3
D_{Cr}^{Opx} EMP	–	3.5 ± 0.99	5.6 ± 2.2	–	4.2 ± 1.1	4.4 ± 1.3	10 ± 4
D_{Cr}^{Opx} SIMS	–	–	–	–	3.4 ± 1.1	6.6 ± 2.1	2.1 ± 0.7
D_{Cr}^{Cpx} EMP	–	–	–	–	–		18 ± 6
D_{Cr}^{Cpx} SIMS	–	–	–	–	–		7.8 ± 2.4
D_{V}^{Ol} SIMS	–	–	–	0.10 ± 0.03	0.11 ± 0.03	0.4 ± 0.1	0.29 ± 0.09
D_{V}^{Opx} SIMS	–	–	–	–	0.7 ± 0.2	1.2 ± 0.4	1.1 ± 0.3
D_{V}^{Cpx} SIMS	–	–	–	–	–	–	1.5 ± 0.5
D_{V}^{Ol}†	–	–	–	0.14 ± 0.04	–	–	–

fO_2 = IW	Eg6		
Temperature	(1250 °C)	(1200 °C)	(1150 °C)
NBO/T	1.26	1.21	1.05
D_{Cr}^{Ol} EMP	0.8 ± 0.1	–	–
D_{Cr}^{Ol} SIMS	0.7 ± 0.2	–	–
D_{Cr}^{Opx} EMP	1.7 ± 0.3	2.8 ± 0.3	3.5 ± 1.2
D_{Cr}^{Opx} SIMS	1.7 ± 0.5	2.8 ± 0.6	3.0 ± 0.9
D_{V}^{Ol} SIMS	0.33 ± 0.11	–	–
D_{V}^{Opx} SIMS	0.9 ± 0.3	1.6 ± 0.4	1.7 ± 0.5
D_{V}^{Ol}†	0.33 ± 0.02	–	–

*Carried out at UNM (all others are experiments at JSC).
†From Canil (1997).

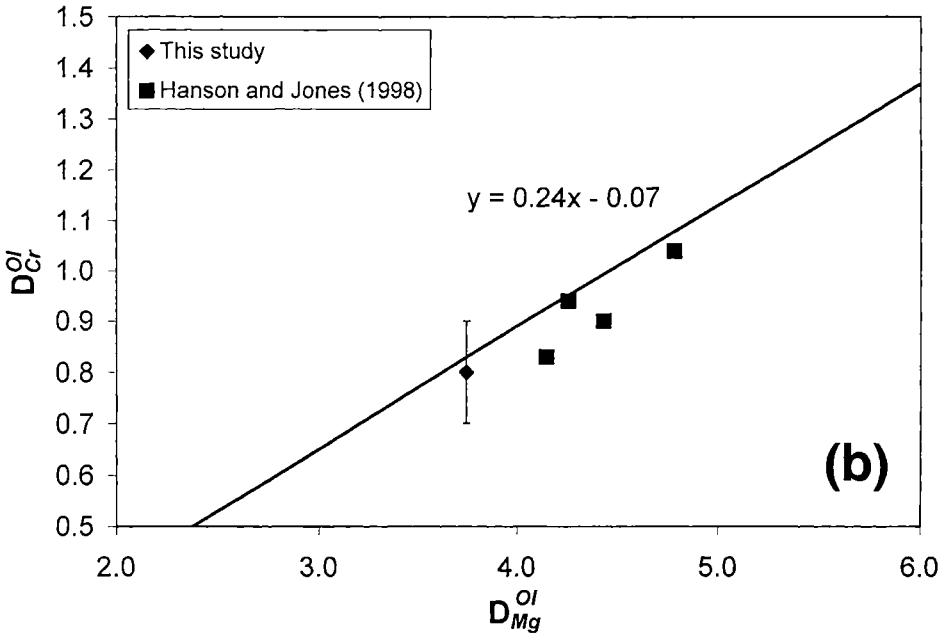

FIG. 4. *Continued.* (b) D_{Cr}^{Ol} *vs.* D_{Mg}^{Ol} from the IW 1250 °C experiment. Also shown are selected data points and the regression line from Hanson and Jones (1998). At IW, most of the Cr is Cr^{2+}.

Jones (1998), thus implying that most of the Cr is Cr^{2+}. This is shown in Fig. 4b, along with some of the data points from Hanson and Jones (1998). These valence assignments, though consistent with earlier work, are not rigorous because of the small change in D_{Cr}^{Ol} with oxygen fugacity. This lack of change is to be expected for some compositional systems with NBO/T near unity (Gaetani and Grove, 1997; Hanson and Jones, 1998).

In contrast to D_{Cr}^{Ol}, the main control on D_V^{Ol} is oxygen fugacity, as shown by Canil (1997) and Hanson and Jones (1997). The D_V^{Ol} values presented here are in good agreement with those given by Canil (1997) and Canil and Fedortchouk (2001), for olivine in komatiite systems (as shown in Fig. 5) despite differences in bulk composition. The D_V values of Canil (1997) are also given in Table 5. D_V^{Ol} is higher at lower oxygen fugacity due to the higher proportion of V^{3+} in the liquid (Canil, 1999), which is more soluble in olivine than V^{4+}.

Chromium and Vanadium Partitioning into Pyroxene–Figure 6a demonstrates that oxygen fugacity also affects the partitioning of Cr into pyroxene. Cr substitutes more readily into orthopyroxene at higher oxygen fugacities, due to the crystal field stabilization of Cr^{3+}. Figure 6b shows the relationship between D_{Cr}^{Px} and D_{MgO}^{Px} at lower oxygen fugacity.

Oxygen fugacity also has an effect on V partitioning in pyroxene. Figure 7 shows the relationship between D_V^{Px} and oxygen fugacity for our experiments and those of Canil (1999). Canil (1999) employed synthetic orthopyroxene-saturated mafic and komatiitic starting compositions and obtained systematically lower D_V^{Opx} values than we did. We suspect that differences in composition are responsible for the differences in the partition coefficients. Canil (1999) noted that a change in the partitioning behavior of V into orthopyroxene, which prefers V^{3+}, occurs at about QFM –2, an oxygen fugacity that is bracketed by the experiments in our study. An indication of this change is seen in the data from our study in Fig. 7. As with V in olivine, the uptake of V is greater in pyroxene at lower oxygen fugacity, as V^{3+} increases.

Implications for the Petrogenesis of Elephant Moraine 79001 Lithology A and the Eg Composition

The compositional overlap between (1) experimental pyroxenes, (2) natural groundmass pigeonite cores, and (3) natural pigeonite rims on orthopyroxene xenocrysts suggests that the rims of the xenocrysts have been modified by either diffusive equilibration with the liquid or by overgrowth from

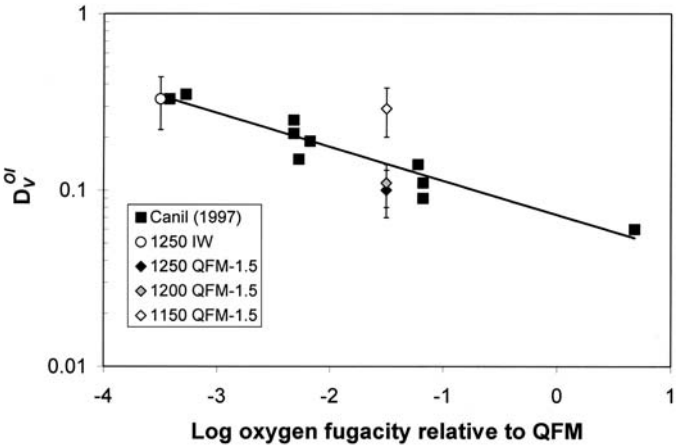

FIG. 5. Relationship between log D_V^{Ol} and oxygen fugacity after Canil (1997), with results from this study.

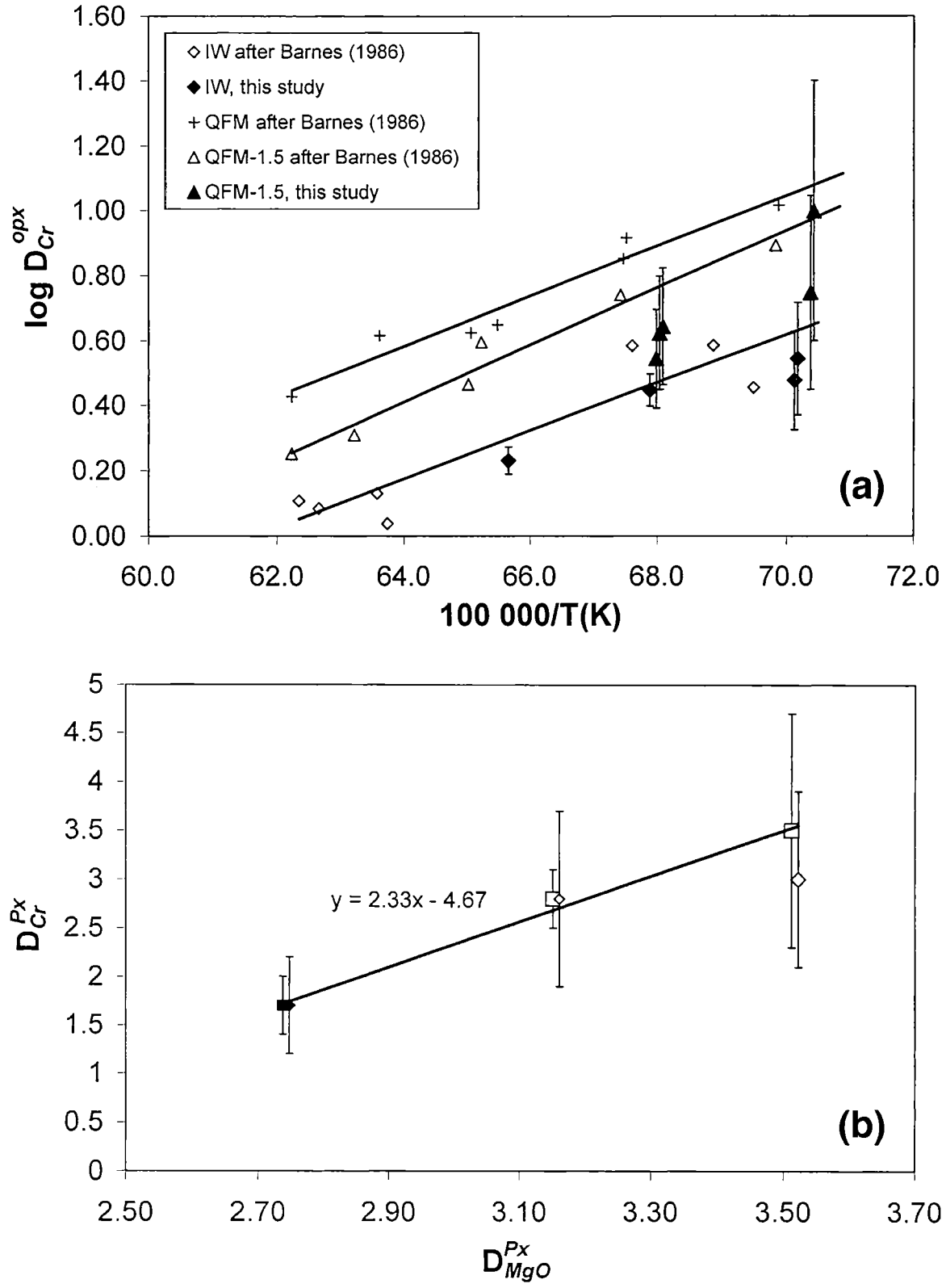

FIG. 6. (a) Partition coefficient data for Cr between low-Ca pyroxene and silicate melt, plotted as log D *vs.* reciprocal temperature for different temperature–fO_2 curves after Barnes (1986), with data from this study for comparison. Data points from this study have been offset slightly for clarity. (b) Plot of D_{Cr}^{Px} *vs.* D_{MgO}^{Px} at IW. Open symbols represent 1150 °C data, gray 1200 °C data (center) and black 1250 °C data. Squares represent EMP data and diamonds SIMS data. Data points have been offset slightly for clarity.

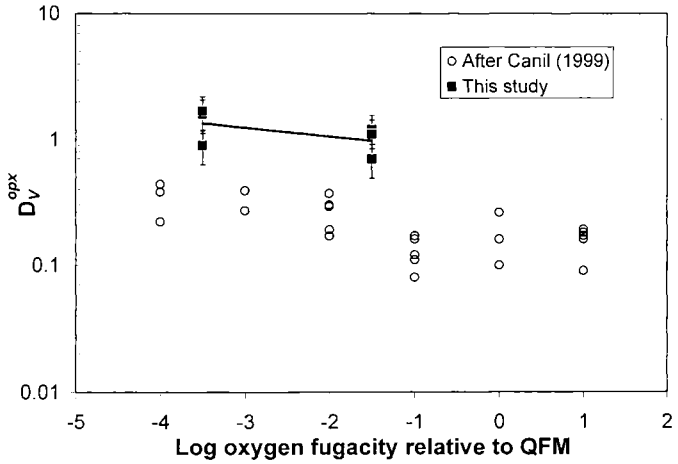

FIG. 7. Plot of D_V^{Opx} *vs.* log fO_2 relative to the QFM buffer for orthopyroxene-liquid partitioning experiments, after Canil (1999), with results from this study (from SIMS data) for comparison. Variation in D_V^{Opx} at a given oxygen fugacity is due to changes in temperature (as temperature decreases, D_V^{Opx} increases).

the same liquid that is now groundmass (Fig. 1). The same could possibly also be true of the Fe-rich rims on xenolithic olivine.

The thicknesses of these olivine rims can be quite variable, even on a single xenolith. Figure 8 shows a map of Fe/Si for an olivine xenocryst from lithology A. In some regions the rim is quite thick and gradually grades into the Mg-rich core. In other areas it is unclear whether there is any real rim at all. In some areas olivines of very different composition appear to be in fault contact and it is not evident that these faults continue into the groundmass. In some areas the Fe-rich rim appears to be in sharp contact with the Mg-rich core. The overall impression is that the zoning and rimming of olivines in lithology A predated their incorporation into the groundmass. In addition, no comparison between olivine rims and groundmass olivines is possible because there is no olivine in the lithology A groundmass.

In contrast, Fig. 9 shows that, in terms of Fe/Si, it is often difficult to discern where pyroxene rim material ends and groundmass pyroxene begins. Pyroxene rims are on the order of 100–200 μm, and are optically distinguishable. In multi-crystal xenoliths, rims are more Fe-rich against the groundmass than at intra-xenolith grain boundaries. Zoning profiles of the Mg-rich cores are flat and wide. Microfaults are also observed in the pyroxene xenoliths, but at least some of these appear to continue into the groundmass.

These observations, coupled with known diffusivities of Fe and Mg in olivine and pyroxene, lead us to believe that the pyroxene rims are overgrowths, not attempts at diffusive equilibration. If diffusive equilibration had occurred, the thickness of the rims on pyroxene would be expected to be much less than those on olivine, because the diffusivity of Fe and Mg in pyroxene is on the order of 10^{-3} less than in olivine (Walker *et al.*, 1977; Schwandt *et al.*, 1998). Conversely, if a significant volume of the pyroxene managed to diffusively equilibrate with the groundmass liquid, then olivine should have completely equilibrated. Therefore, we do not believe that either the olivine or pyroxene rims formed by diffusion. Pyroxene rims may, therefore, have formed by overgrowth, but olivine rims appear to have formed before incorporation into lithology A.

In order to test this idea, we analyzed Cr and V in the olivine and pyroxene rims using SIMS. These, along with our experimentally-determined D values, were then used to calculate the concentrations of Cr and V in the liquid the rims crystallized from. Table 6 gives concentrations of Cr and V in the olivine and pyroxene xenocryst rims, as well as in pyroxene cores from the groundmass. Cr and V concentrations in the

TABLE 6. Comparison of V and Cr in rims of xenocrystic orthopyroxene and olivine with cores of low-Ca pyroxene in the groundmass.

	V in xenocryst rim* (ppm)	V in groundmass* (ppm)	Cr in xenocryst rim* (ppm)	Cr in groundmass* (ppm)
Olivine	17 ± 3	n/a§	315 ± 110	n/a§
Liquid *mg#*	0.30	–	0.30	–
D value†	0.3 ± 0.1	–	1.0 ± 0.3	–
Liquid concentration‡	59 ± 21	–	315 ± 145	–
Pyroxene	224 ± 38	177 ± 17	3644 ± 502	3313 ± 342
Liquid *mg#*	0.34	0.40	0.34	0.40
D value†	1.1 ± 0.3	1.1 ± 0.3	2.1 ± 0.7	2.1 ± 0.7
Liquid concentration‡	204 ± 65	161 ± 47	1735 ± 626	1578 ± 551

*Average of several grains.

†Chosen based on experiments performed at QFM –1.5 (see Table 5).

‡Calculated from $C_{melt} = C_{mineral}/D$.

§No olivine has been found in the groundmass in EET 79001 lithology A.

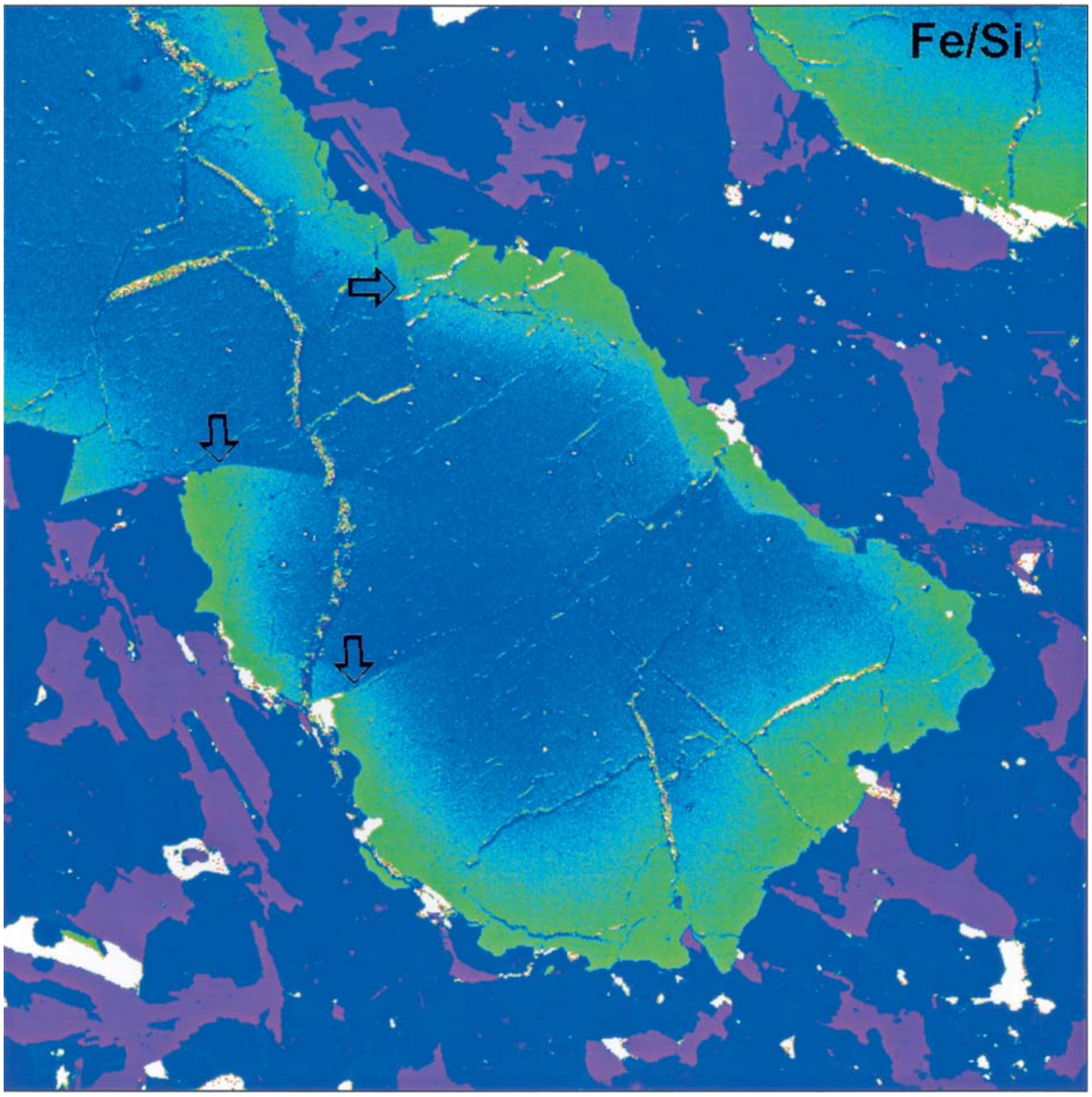

FIG. 8. Fe/Si element ratio map of an olivine xenocryst in lithology A of thin section EET 79001,68. The image is 800 × 800 pixels with each pixel being 2 μm on a side. Iron-rich rims of the olivine are disrupted by microfaults which do not continue into the groundmass (shown by arrows). Olivine rim compositions are not affected by groundmass pyroxene compositions and vice versa.

coexisting liquids are calculated from *D* values derived from 1150 °C runs, which have *mg#* close to those calculated for the natural olivine and pyroxene compositions. The xenocryst pyroxene rim compositions and the groundmass pyroxene compositions for Cr and V agree within error, further indicating that the pyroxene rims may in fact be overgrowths. Liquid compositions calculated from our pyroxene *D* values, therefore also agree. However, Cr and V concentrations in the liquid calculated from olivine rims do not agree with those calculated using xenocryst rim or groundmass pyroxene. Chromium in the liquid calculated from olivine rims is a factor of 5 lower than Cr calculated using pyroxene analyses. Vanadium in the liquid calculated from olivine rims is a factor of 3 lower than V calculated using pyroxene analyses. We conclude that both petrography and trace element analysis support the hypothesis that the olivine rims are autochthonous to the xenocrysts. These results also support the hypothesis that the olivine megacrysts are xenocrystic, because olivine rims with such a low concentration of Cr and V (Table 6) could not form from the groundmass melt.

If the xenocryst pyroxene rims are indeed indigenous to the groundmass, then the Eg composition requires modification. The subtractive method used by McSween and Jarosewich (1983) to establish Eg could not have resulted in a totally

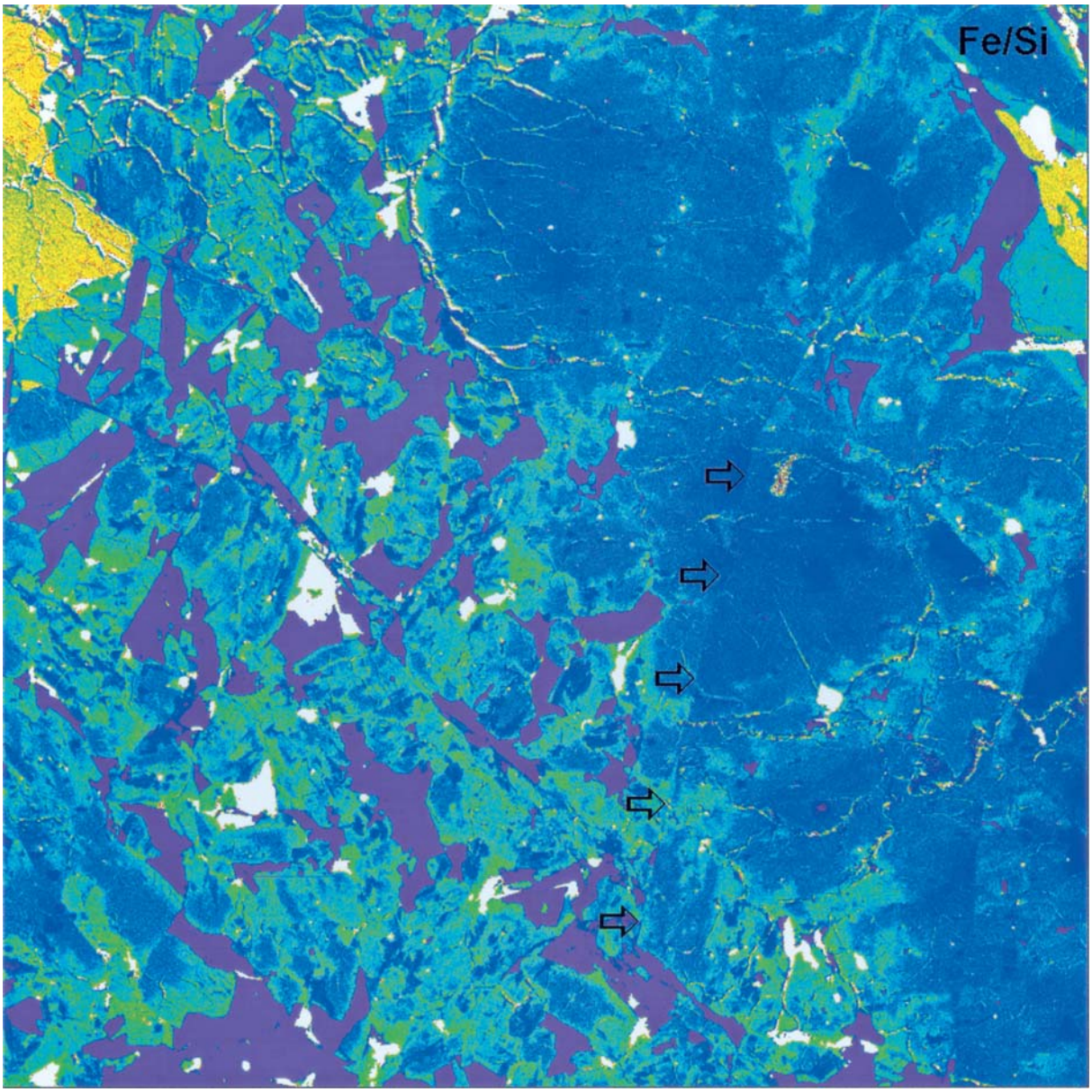

FIG. 9. Fe/Si element ratio map of a pyroxene xenocryst in lithology A of thin section EET 79001,68. The image is 1000 × 1000 pixels with each pixel being 2 μm on a side. Mottling (due to slight compositional variations) of xenocryst rims is indistinguishable from the mottling of groundmass pyroxene rims. Microfaults can be traced from the interiors of the xenocrysts into the groundmass (shown by arrows).

accurate representation of the groundmass composition because they subtracted the average of olivine and pyroxene xenocryst core and rim compositions. We believe this is the correct procedure for olivine xenoliths but not for pyroxene xenoliths, whose rims were probably not a part of the xenolith at the time it was incorporated into the lithology A liquid.

Based on our observations, it is likely that the true Eg composition is more pyroxene normative than that of Longhi and Pan (1989). Conceivably, therefore, this could account for the discrepancy between the lack of olivine observed in the groundmass and the presence of olivine in experimental runs (Longhi and Pan, 1989; Wasylenki *et al.*, 1993). We present our initial best estimate of the Eg composition in Table 1. This was made by modifying the estimate of Schwandt *et al.* (2001), by including an estimate of the proportion of overgrowth material in a single pyroxene xenocryst, using optical means on section EET 79001,73. Therefore, the Eg composition presented in Table 1 reflects the observation that ~30% of the pyroxene xenocrysts are indigenous to the groundmass. This composition is appropriately less olivine normative than previous estimates. We note, however, that this is a preliminary result; ideally, the pyroxene overgrowth material should be distinguished by optical means in conjunction with other methods (Schwandt *et al.*, 2001) on a

number of pyroxene xenocrysts to obtain a statistically significant estimate of the amount of overgrowth material.

Acknowledgements–The authors thank David Mittlefehldt and Allan Treiman for discussions of the Cr content and the petrogenesis of EET 79001 lithology A. Loan Le and Rhian Jones helped with the experiments at the Johnson Space Center and University of New Mexico, respectively. We also thank Chip Shearer and Justin Hagerty for help with SIMS analyses. Thin sections were provided by the Antarctic Meteorite Program (NASA Johnson Space Center). This project was funded by the NASA Graduate Student Researchers Program (NGT-931 to J. J. P.; awarded to C. D. K. H.), the NASA "Microbeam Studies of Planetary Materials" Grant MRA 97-282 to J. J. P., RTOP 344-31-20-18 to J. H. J., and the Institute of Meteoritics. This manuscript benefited greatly from reviews by Hap McSween and John Longhi. This paper represents LPI Contribution 1125.

Editorial handling: H. Nagahara

REFERENCES

BARNES S. J. (1986) The distribution of chromium among orthopyroxene, spinel and silicate liquid at atmospheric pressure. *Geochim. Cosmochim. Acta* **50**, 1889–1909.

BORISOV A. AND JONES J. H. (1999) An evaluation of Re, as an alternative to Pt, for the 1 bar loop technique: An experimental study at 1400 °C. *Am. Mineral.* **84**, 1528–1534.

CANIL D. (1997) Vanadium partitioning and the oxidation state of Archean komatiite magmas. *Nature* **389**, 842–845.

CANIL D. (1999) Vanadium partitioning between orthopyroxene, spinel and silicate melt and the redox states of mantle source regions for primary magmas. *Geochim. Cosmochim. Acta* **63**, 557–572.

CANIL D. AND FEDORTCHOUK Y. (2001) Olivine-liquid partitioning of vanadium and other trace elements, with applications to modern and ancient picrites. *Can. Mineral.* **39**, 319–330.

GAETANI G. A. AND GROVE T. L. (1997) Partitioning of moderately siderophile elements among olivine, silicate melt, and sulfide melt: Constraints on core formation in the Earth and Mars. *Geochim. Cosmochim. Acta* **61**, 1829–1846.

GROVE T. L. AND BENCE A. E. (1977) Experimental study of pyroxene-liquid interaction in quartz-normative basalt 15597. *Proc. Lunar Sci. Conf.* **8th**, 1549–1579.

HANSON B. Z. AND JONES J. H. (1997) The contrasting partitioning behavior of V and Cr into olivine (abstract). *EOS* **78 (Suppl.)**, S335.

HANSON B. Z. AND JONES J. H. (1998) The systematics of Cr^{3+} and Cr^{2+} partitioning between olivine and liquid in the presence of spinel. *Am. Mineral.* **83**, 669–684.

HERD C. D. K., PAPIKE J. J. AND BREARLEY A. J. (2001) Oxygen fugacity of martian basalts from electron microprobe oxygen and TEM-EELS analyses of Fe-Ti oxides. *Am. Mineral.* **86**, 1015–1024.

JUREWICZ A. J. G., WILLIAMS R. J., LE L., WAGSTAFF J., LOFGREN G., LANIER A., CARTER W. AND ROSHKO A. (1993) *Technical Update: JSC System Using a Solid Electrolytic Cell in a Remote Location to Measure Oxygen Fugacities in CO/CO_2 Controlled-Atmosphere Furnaces*. NASA Technical Memorandum **104774**, NASA, Houston, Texas, USA. 39 pp.

LONGHI J. AND PAN V. (1989) The parent magmas of the SNC meteorites. *Proc. Lunar Planet. Sci. Conf.* **19th**, 451–464.

MCSWEEN H. Y., JR. AND JAROSEWICH E. (1983) Petrogenesis of the Elephant Moraine A79001 meteorite: Multiple magma pulses on the shergottite parent body. *Geochim. Cosmochim. Acta* **47**, 1501–1513.

MEYER C. (1998) *Mars Meteorite Compendium–1998*. NASA Johnson Space Center, Houston, Texas, USA. 237 pp.

MITTLEFEHLDT D. W., LINDSTROM D. J., LINDSTROM M. M. AND MARTINEZ R. R. (1999) An impact melt origin for lithology A of martian meteorite Elephant Moraine 79001. *Meteorit. Planet. Sci.* **34**, 357–367.

MYSEN B. O. (1983) The structure of silicate melts. *Ann. Rev. Earth Planet. Sci.* **11**, 75–97.

SCHWANDT C. S., CYGAN R. T. AND WESTRICH H. R. (1998) Magnesium self-diffusion in orthoenstatite. *Contrib. Mineral. Petrol.* **130**, 390–396.

SCHWANDT C. S., JONES J. H., MITTLEFEHLDT D. W. AND TREIMAN A. H. (2001) The magma composition of EET79001A: The first recount (abstract). *Lunar Planet. Sci.* **32**, #1913, Lunar and Planetary Institute, Houston, Texas, USA (CD-ROM).

STEELE I. M. AND SMITH J. V. (1982) Petrography and mineralogy of two basalts and olivine-pyroxene-spinel fragments in achondrite EETA79001. *Proc. Lunar Planet. Sci. Conf.* **13th**, *J. Geophys. Res.* **87**, A375–A384.

WADHWA M., MCSWEEN H. Y., JR. AND CROZAZ G. (1994) Petrogenesis of shergottite meteorites inferred from minor and trace element microdistributions. *Geochim. Cosmochim. Acta* **58**, 4213–4229.

WALKER D., KIRKPATRICK R. J. AND HAYS J. F. (1976) Crystallization history of lunar picritic basalt sample 12002: Phase-equilibria and cooling-rate studies. *Geol. Soc. Am. Bull.* **87**, 646–656.

WALKER D., LONGHI J., LASAGA A. C., STOLPER E. M., GROVE T. M. AND HAYS J. F. (1977) Slowly cooled microgabbros 15555 and 15065. *Proc. Lunar Sci. Conf.* **8th**, 1521–1547.

WASYLENKI L. E., JONES J. H., LE L. AND JUREWICZ A. J. G. (1993) Equilibrium and fractional crystallization of a primitive shergottite composition (abstract). *Lunar Planet. Sci.* **24**, 1491–1492.

WONES D. R. AND GILBERT M. C. (1969) The fayalite–magnetite–quartz assemblage between 600 and 800 °C. *Am. J. Sci.* **267A**, 480–488.